Supplementary Information (SI) for Environmental Science: Processes & Impacts.
This journal is © The Royal Society of Chemistry 2026

Supporting information

Colloidal stability and aggregation of polyethylene (PE) nanoplastics under UV weathering and PFOA contamination

Peiyao Wu[1], Marina Pasquet[1,3], Vy Duong[1], Viktoriia Riabchenko[1], Joelle Frechette[1,2]

1.Chemical and Biomolecular Engineering Department, University of California, Berkeley CA, 94720, USA, 2. Energy Conversion Group, Lawrence Berkeley National Laboratory, Berkeley CA, 94720, USA, 3. Biofisika Institute (CSIC, UPV/EHU) and Department of Biochemistry and Molecular Biology, University of the Basque Country, Leioa, 48940, Spain.

Corresponding author: Joelle Frechette, jfrechette@berkeley.edu

1. Additional FT-IR spectra after 90 h and 180 h weathering treatment.

FT-IR measurements were conducted after PE sheets underwent weathering treatment of 0 h (main **Fig. 1D**), 90 h (**Fig. S1A**), 180 h (**Fig. S1B**), 300 h (main **Fig. 2A**). We have zoomed in on region $1300-1850\ cm^{-1}$ and plotted them as insets in each spectrum. After 90 h treatment, the areas between $1650-1850\ cm^{-1}$ (C=O stretching) are much larger for PE particles and sheets in water than in air (**Fig. S1A**). In contrast, after 180 h treatment, the same area has a similar magnitude for all 4 conditions (**Fig. S1B**). The CI were calculated from these spectra and plotted in the main text **Fig 1B**. Methods for calculating CI varies, and literature comparison[1] showed the specified area under bands worked best for a large range of polymer samples. To ensure an effective comparison, spectra were scaled by peak around $2914\ cm^{-1}$ and baselines were adjusted to be the same for $1550-1630\ cm^{-1}$ across all spectra. Then an integration algorithm using Simpson's rule from scipy library was implemented for the designated region and used here for calculating CI according to:

$$Carbonyl\ index\ (CI) = \frac{Integration\ of\ C=O\ peak\ (1650\ -1850\ cm^{-1})}{Integration\ of\ CH_2\ scissoring\ peak\ (1420\ -1500\ cm^{-1})}.\#(S1)$$

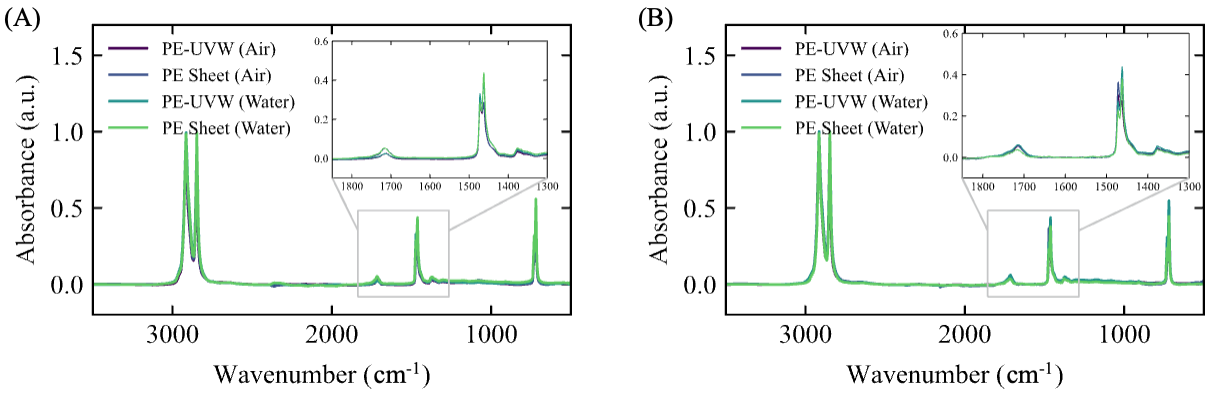

Fig. S1. FT-IR spectra for particles and sheets after (A) 90 h and (B) 180 h weathering treatment either in water or in air, with the region of $1850-1300\ cm^{-1}$ zoomed in.

2. Weathering reaction schemes

a. UV weathering reaction scheme in air

In air the reaction will be dominated by β-scission and H-abstraction. Literature data shows lower molecular weight and a small amount of either ozone or H_2O_2 generated from UV radiation:[2]

$$\left[-CH_2-CH_2-\right]_n \xrightarrow{h\nu} \left[-CH_2-\right]_n CH_2\cdot + \left[-CH_2-\right]_n CH_2\cdot + 2\,H\cdot \quad \#(S2)$$

$$\left[-CH_2-\right]_n CH_2\cdot + O_2 \rightarrow \left[-CH_2-\right]_n COOH + H\cdot \quad \#(S3)$$

$$2H\cdot + O_2 \rightarrow H_2O_2 \quad \#(S4)$$

b. UV weathering reaction scheme in water

Samples weathered in water should undergo the same scission and abstraction as the in-air schemes, but also an additional pathway might exist based on literature evidence[3] regarding a small amount of radicals generated from water under UV. We hypothesize the PE in water undergoes reactions in this sequence:

$$H_2O \xrightarrow{h\nu} H\cdot + \cdot OH \#\#(S5)$$

$$\cdot OH + \cdot OH \leftrightarrow H_2O_2 \quad \#(S6)$$

$$\left[-CH_2-CH_2-\right]_n + \cdot OH \rightarrow \left[-CH_2-CH_2-\right]_{n-x} - OH + \left[-CH_2-CH_2-\right]_x\cdot \quad \#(S7)$$

$$\left[-CH_2-CH_2-\right]_x\cdot + \cdot OH + O_2 \rightarrow R-COOH + R-OH + CO_2 + H_2O \quad \#(S8)$$

3. Particle number density calculation using Mie theory

In the Mie scattering regime, we can calculate concentration of particles using a series of equations with calculated Mie scattering cross section and measured absorbance from UV-vis.[4,5] The Mie cross section C_{sca} is calculated as:

$$C_{sca} = \frac{2\pi}{k^2}\sum_{n=1}^{\infty}(2n+1)\left(|a_n|^2 + |b_n|^2\right) \quad \#(S9)$$

$$a_n = \frac{x j_n(x)\left[mx\, j_n(mx)\right]' - m^2 x\left[x\, j_n(x)\right]' j_n(mx)}{x h_n(x)\left[mx j_n(mx)\right]' - m^2 x\left[x h_n(x)\right]' j_n(mx)} \quad \#(S10)$$

$$b_n = \frac{mx j_n(x)\left[mx\, j_n(mx)\right]' - mx\left[x\, j_n(x)\right]' j_n(mx)}{mx h_n(x)\left[mx j_n(mx)\right]' - m^2 x\left[x h_n(x)\right]' j_n(mx)} \quad \#(S11)$$

Here, j_n is the spherical Bessel function of the first kind, and h_n is the spherical Hankel function of the first kind. The other parameters are $m = n_{particle}/n_{medium}$, $k = \frac{2\pi n_{medium}}{\lambda}$, $x = ka$. The number density of particles is calculated using Beer Lambert Law and Lorentz-Mie theory[4] as:

$$n_0 = \frac{2.303\, A_{450}}{C_{sca}} \quad \#(S12)$$

Here, A_{450} is the absorbance measured at a relatively large wavelength 450 nm using UV-vis. The resulting number density is in unit of # particles/volume.

4. Aggregation rate constant and stability ratio calculation

According to Rayleigh-Gans-Debye theory,[5,6] in an aggregation process one can consider a doublet as a sphere with the same volume and apply Mie theory to this sphere if the primary particles are relatively small compared to the incident wavelength. This theory is used in combination with experimental techniques using scattering to evaluate the singlet to doublet aggregation kinetics. In addition, this approach is only valid if the colloid system satisfies $kd * |m-1| = \frac{2\pi d}{\lambda} * |\frac{n_{particle}}{n_{medium}} - 1| \ll 1$, with n being the refractive index of the corresponding species.

For our system, we have $\frac{2\pi d}{\lambda} * \left|\frac{n_{particle}}{n_{medium}} - 1\right| = 0.25 < 1$, meaning that it is reasonable to use this approximation. RGD has been used routinely to calculate an optical factor in combination with DLS data to quantify aggregation kinetics with a stability ratio (W) or attachment efficiency frameworks.[7–9] This optical factor is usually expressed as $o=\left[\frac{\sin(2r_0q)}{2r_0q}+1\right]\left(1-\frac{r_{h1}}{r_{h2}}\right)$. Using this approximation with size change over time obtained from DLS, we can calculate an aggregation constant for each experiment.

The main equation is now:

$$k_{slow} = \frac{1}{r_0 * (o) * n_0}\left[\frac{d\,r(t)}{d\,t}\right]_{t\to 0} \#(S13)$$

With the variables defined in the main text. Our evaluation of the applicability of RGD is consistent with the range used in the literature. For example, Holthoff H. et al (1997) used RGD approximation to calculate an optical parameter $I_2/(2\,I_1)$ for similar sized (200 nm diameter) PS particles and compared it to the SLS result, showing the values are similar. We obtain the exact same function as the calculated result in Holthoff, confirming that the approximation is valid for our parameters and that we can either measure or calculate $I_2/(2\,I_1)$.

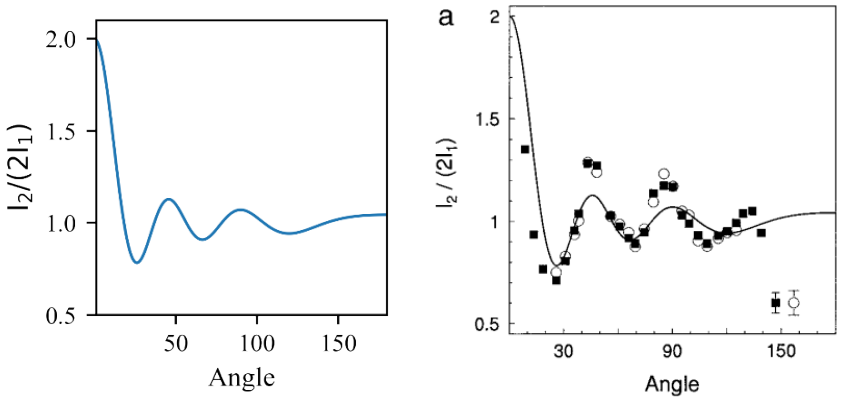

Figure S2. [Left] Our calculation of $I_2/(2\,I_1)$ using radius and wavelength from Holthoff 1997, [right] calculations (lines) and SLS result (dots) comparison from Holthoff 1997

Note: The attachment efficiency α is the inverse stability ratio,[9] and our conclusions regarding the stability trend remain the same regardless of whether α or W is used in the discussion:

$$\alpha = \frac{1}{W} = \frac{k_{slow}}{k_{fast}} \#(S14)$$

5. Quantification of PFOA adsorption using interfacial tension measurements.

We rely on interfacial tension (IFT) measurements to capture the depletion of PFOA in the bulk caused by adsorption to PE particles. IFT offer the sensitivity needed to effectively monitor the depletion of bulk PFOA due to its adsorption onto PE particles. Below the critical micelle concentration, the extent of PFOA adsorption to the air-water interface increases with the concentration of PFOA in the bulk aqueous phase. As PFOA adsorbs to PE particles, the bulk PFOA concentration decreases and the interfacial tension increases. A mass balance allows us to calculate the PFOA adsorbed on particles from the PFOA depleted in the bulk aqueous phase.

To evaluate the amount of PFOA adsorbed onto surface of PE NPs, 700 nm diameter PE NPs with $n_0 \approx 5 \times 10^{16} - 7 \times 10^{16}\ \#/m^3$ were incubated under various PFOA concentrations (same incubation conditions as 200 nm PE-PFOA studied). We selected larger particles to characterize adsorption because their diffusion timescale to the air-water interface is significantly longer such that particle attachment to the air-water interface do not occur at comparable time scales than PFOA adsorption. After incubation and before IFT measurement, the dispersions were centrifuged at 14000 rpm for 40 minutes and the particle-free bottom liquid was extracted for tensiometry. The equilibrium IFT values were recorded for both PFOA-only (γ_1) and PE-PFOA leftover liquid (γ_2) versus different initial concentrations. Representative IFT dynamics data are shown in **Fig. S3A for** $\gamma_1(t)$ and $\gamma_2(t)$. The resulting interfacial tension isotherm is shown in **Fig. S3B**. The bulk concentration in **Fig. S3B** is corrected for loss due to adsorption to PE.

We fit the interfacial tension isotherm for PFOA-only $\gamma_1(C_{b,eq})$, to a Szyszkowski-Langmuir equation (**Equation (S9)**) and obtain two fitting parameters for PFOA adsorbing to air-water interface: $\Gamma_{aw,max}$ and $K_{aw,ad}$. Here $C_{b,eq}$ is the bulk PFOA concentration, γ_0 is the surface tension of DI water, and we assume $C_{b,i} \approx C_{b,eq}$ for PFOA-only solutions ($C_{b,i}$ being the initial PFOA bulk concentration at the start of incubation). For this and following equation we use N/m for γ and mM for C_{beq}:

$$\gamma_1 = \gamma_0 - RT\,\Gamma_{aw,max} \ln\left(1 + K_{aw,ad} C_{b,eq}\right). \#(S15)$$

The best fit for this function using our experimental data is: $\Gamma_{aw,max} = 3.06 \times 10^{-6}\ mol/m^2$, and $K_{aw,ad} = 25.15$. We can rewrite **Equation (S9)** to be:

$$C_{b,eq} = \frac{1}{K_{aw,ad}} \cdot \left[\exp\left(\frac{\gamma_0 - \gamma_1}{RT\,\Gamma_{aw,max}}\right) - 1\right]. \#(S16)$$

We use this equation to fit the bulk PFOA as well as the depleted bulk PFOA after adsorption to PE (γ_2) using the same parameters. The total amount (in mol) lost from the bulk solution is $(C_{b,i}V - C_{b,eq}V)$. We then estimate the surface excess Γ_p of PFOA on the surface of PE NPs by using a mass balance assuming that all PFOA depleted from the bulk is due to adsorption onto the surface of the PE particles:

$$C_{b,i}V - C_{b,eq}V = \Gamma_p A_p \,. \#(S17)$$

Here, V is the volume of total particle solutions in a vial after incubation (usually about 6 mL), and A_p is the total surface area of all particles in that volume (calculated using known diameter 700 nm and number density $n_0 \approx 5 \times 10^{16} \sim 7 \times 10^{16}\ \#/m^3$). In main text, **Fig. 3** shows the calculated and modeled Γ_p vs. $C_{b,eq}$

using the Langmuir adsorption isotherm (written in terms of surface excess) assuming the PFOA molecules are limited to a monolayer on PE surface:

$$\Gamma_p = \frac{\Gamma_{p,\,max} \cdot K_{p,ad} \cdot C_{eq}}{1 + K_{p,ad} \cdot C_{eq}} .\#(S18)$$

Γ_p is in unit of mol/area on the PE surface, and the two parameters we used are $\Gamma_{p,max} = 3.21 \times 10^{-6}\, mol/m^2$ and $K_{p,ad} = 1.46$.

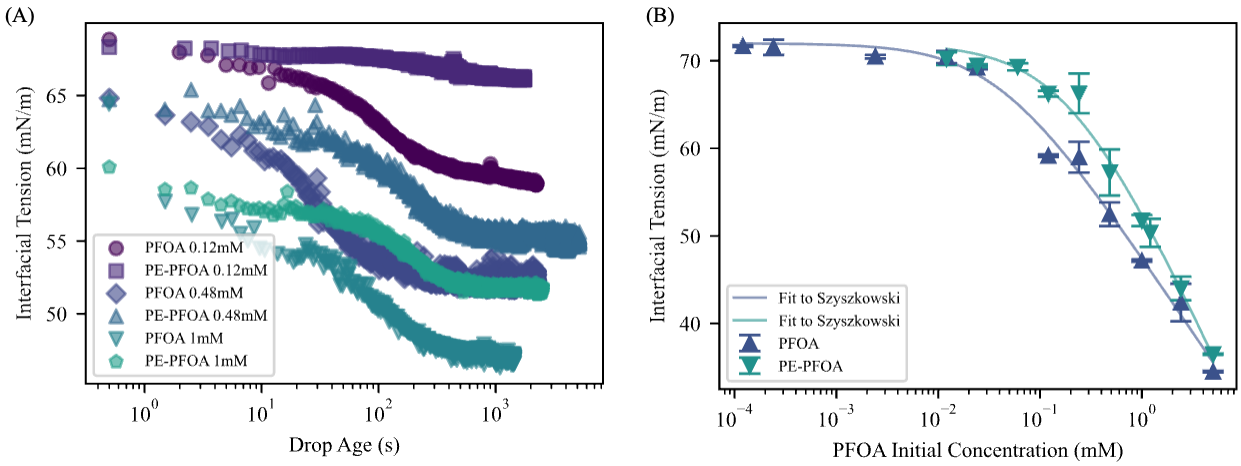

Fig. S3. (A) Interfacial tension (IFT) dynamics data obtained for only PFOA solution and PE-PFOA solution after incubation with PE particles removed, with respective initial [PFOA] of 0.12 mM, 0.48 mM, 1 mM. (B) equilibrium IFT obtained from a series of experiments including the ones shown in (A) over different initial concentration, with a fit to Szyszkowski-Langmuir equation.

6. DLVO and XDLVO theory calculations

The net interaction potential between two particles (Φ_{net}) is calculated as the sum of van der Waals (Φ_{vdW}) and electrostatic double layer (Φ_{DL}) interactions potentials for a separation distance S_0 based on DLVO theory:

$$\Phi_{net}(S_0) = \Phi_{vdW}(S_0) + \Phi_{DL}(S_0).\#(S19)$$

We calculate the van der Waals interaction potential for two identical spheres of radius r using:[10]

$$\Phi_{vdW} = -\frac{A \cdot r}{12\, S_0}.\#(S20)$$

where, r is the sphere radius, S_0 is the separation distance between the two sphere surfaces at the closest point, such that the center-to-center distance between two spheres is $(S_0 + 2\,r)$, and A is the Hamaker constant calculated using an approximation of Lifshitz theory for the case of two identical spheres interacting across a medium:[11]

$$A = \frac{4}{3}kT\left(\frac{\varepsilon_1 - \varepsilon_3}{\varepsilon_1 + \varepsilon_3}\right)^2 + \frac{3h\nu_e}{16\sqrt{2}} \cdot \frac{\left(n_1^2 - n_3^2\right)^2}{\left(n_1^2 + n_3^2\right)^2}.\#(S21)$$

We use $\varepsilon_1 = 2.25$ and $\varepsilon_3 = 78.4$ for the dielectric constants of polyethylene and water, respectively, and use $n_1 = 1.50$ and $n_3 = 1.33$ for the refractive index of polyethylene and water, respectively.[11] The value for absorption frequency employed is $\nu_e \approx 3 \times 10^{15}\, s^{-1}$ selected for hydrocarbon. The calculated Hamaker constant is then $A = 1.02 \times 10^{-20}\, J$.

The electrostatic double layer (DL) interaction energy is obtained by numerically solving the Poisson-Boltzmann equation for the surface potential distribution between two flat plates in 1-dimension for a 1:1 symmetric electrolyte, and given by:[12]

$$\frac{d^2\psi}{dx^2} = \left(\frac{2zen_\infty}{\varepsilon_0\varepsilon}\right)\sinh\left(\frac{ze\psi}{kT}\right).\#(S22)$$

Here, $\psi(x)$ is the local electrostatic potential at position x between the plates, n_∞ is the ionic number density in the bulk, $e = 1.602 \times 10^{19}\, C$ is the elementary charge, $z = 1$ for a monovalent electrolyte, ε is the permittivity of vacuum, k is Boltzmann constant, and T is the temperature. Then we also set the boundary conditions to be either constant charge (S23) or constant potential (S24):

$$\left(\frac{d\psi}{dx}\right)_{x=0} = -\frac{\sigma_0}{\varepsilon_0\varepsilon} = constant\ .\#(S23)$$

$$\psi(x=0) = \psi_s = constant\ .\#(S24)$$

Symmetry also requires that $\left(\frac{d\,\psi}{d\,x}\right)_{x=\frac{S_0}{2}} = 0$. The system of equations is then solved using python function "solve_bvp" from the scipy library to obtain the potential at any location between the plates, and especially the midplane potential ψ_m for each separation distance S_0. An analytical result for 1:1 electrolyte obtained by Verwey and Overbeek for the force/area (pressure) between two charged plates with separation distance S_0 is:[13]

$$P_x(S_0) - P_x(\infty) = kTn_\infty\left[\exp\left(-\frac{e\psi_m}{kT}\right) - 1 + \exp\left(\frac{e\psi_m}{kT}\right) - 1\right] = 2kT\, n_\infty\left[\cosh\left(\frac{e\psi_m}{kT}\right) - 1\right].\#(S25)$$

The pressure between the plates is the derivative of the interaction energy per unit area, therefore $P_x(S_0) = -\frac{d\Phi}{d\,S_0}$. Along with the boundary condition that $P_x(\infty) = 0$ we can integrate the pressure to obtain the interaction energy between the two flat plates such as:[13]

$$\Phi_{R,flat\ plate}(S_0) = -\int_\infty^D P_x(S_0)dS_0\ .\#(S26)$$

We then use the Derjaguin approximation to obtain the interaction potential between spheres (identical radii in our case):[14]

$$F_{R,\,sph-sph} = 2\pi\left(\frac{R_1R_2}{R_1+R_2}\right)\Phi_{R,\,flat\ plate}(S_0)\ .\#(S27)$$

In **Equation (S27)**, R_1 and R_2 are the radii for sphere 1 and 2, and S_0 is the same separation of distance for the closest points between two spheres. We then obtain the electrostatic interaction potential between spheres by integrating the force between two identical spheres:

$$\Phi_{R,\,sph-sph} = \int_{S_0}^{\infty} F_{R,sph-sph}(S_0)dS_0 \,.\#(S28)$$

The electrostatic interaction potential between two spheres $\Phi_{R,sph-sph}(S_0)$ is written as Φ_{DL} in the main text. From the superposition of Φ_{vdW} and Φ_{DL} using Equation (S19) we obtain a series of total interaction potential energy as a function of separation distance for two spheres across all salt concentrations investigated, as shown in **Fig. S4**.

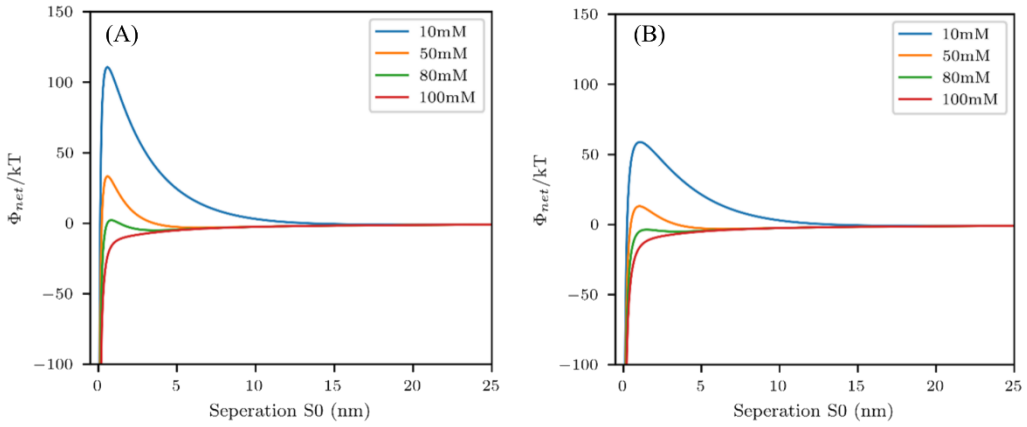

Fig S4. DLVO potential energy prediction for different NaCl salt concentration using zeta potential as measured in experiments, and $A = 1.02 \times 10^{-20}\,J$, diameter of 200 nm. (A): constant charge BC; (B): constant potential BC.

The stability ratio W is calculated for each net interaction potential $\Phi_{net}(u)$ following:[12]

$$W = \frac{k_{fast}}{k_{slow}} = 2r\int_{2r}^{\infty} \frac{\exp\left(\frac{\Phi_{net}(u)}{kT}\right)}{u^2} du \,.\#(S29)$$

In **Equation (S29),** Φ_{net} is the total DLVO interaction potential, and u is the center-to-center separation distance where $u = S_0 + 2r$.

Incorporating hydrophobic interactions using XDLVO theory

In the case of the extended DLVO or XDLVO theory that incorporates with hydrophobic interactions, the interaction potential becomes:

$$\Phi_{net} = \Phi_{vdW} + \Phi_{DL} + \Phi_{hydrophobic} \,\#(S30)$$

Hydrophobic interaction is a short-ranged attractive non-DLVO force and often takes the form of an exponential related to separation distance for a sphere-flat plate geometry:[15,16]

$$\left(\frac{F}{R}\right)_{flat-sph} = -A\exp\left(-qS_0\right) \#(S31)$$

Based on literature reports for other hydrophobic polymers interacting in water the magnitude of A is approximated as $100\ mN/m$ and decay length q^{-1} as 1 nm.[15] Although the exact values might vary for PE, the formulation and signs should remain similar. Thus, the hydrophobic force between two spheres of radius R_1 and R_2 will be:

$$F_{sph-sph} = R_{eff} * \left(-A\exp\left(-qS_0\right)\right) = \frac{R_1R_2}{R_1+R_2} * \left(-A\exp\left(-qS_0\right)\right) \#(S32)$$

Integrating the sphere-sphere interaction force, we can obtain the interaction potential energy $\Phi_{sph-sph}$:

$$\Phi(S_0) = -\int_{\infty}^{S_0} \frac{R}{2} * \left(-A\exp\left(-qS_0\right)\right) dS_0 = A * \frac{R}{2} * \left(-\frac{1}{q}\right)\exp\left(-qS_0\right) - 0 \#(S33)$$

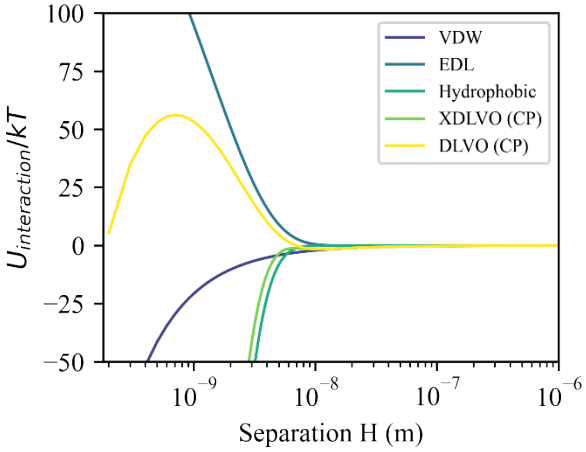

Fig S5. An example of XDLVO with different interactions plotted here for PE-Pristine 200 nm diameter at 30 mM NaCl concentration with $\zeta = -42\ mV$ showing a decrease in total interaction energy with hydrophobic interaction addition compared with DLVO under constant potential (CP) boundary condition.

7. Error analysis of stability data

Starting from:

$$W = \frac{k_{fast}}{k_{slow}} = k_{fast}n_0r_h(0,q)\frac{1}{\left[\frac{d\,r_h(t)}{dt}\right]_{t\to 0}}o\ ,\#(S34)$$

we simplify **Equation (S34)** by defining: $u = \left[\frac{d\,r_h(t)}{dt}\right]_{t\to 0}$, $v = r_h(0)$, and $b = k_{fast}n_0o \approx (6.2\times10^{-18})\ m^3/s\ (4\times10^{14})\ \#/m^3(0.24)$, and rewrite **Equation (S34)** to be:

$$W = b \times \frac{v}{u} \#(S35)$$

The error propagation is then:

$$\frac{\sigma_w^2}{W^2} = \frac{\sigma_u^2}{u^2} + \frac{\sigma_v^2}{v^2} \#(S36)$$

Here, we have $\sigma_v^2 = PDI * mean^2$ and $\sigma_u^2 = SE^2 * n.$ The standard error (SE) in σ_u will be from the linear regression error when we fit a linear function to r(t) vs. time, and n is the number of particles sampled in each measurement using n_0 times the volume the laser passes through in the DLS cuvette. With propagation we arrive at the final variance in W:

$$\sigma_w^2 = W^2 * \left(\frac{SE^2 * n}{u^2} + PDI * \frac{r_0^2}{r_0^2} \right), \#(S37)$$

and then we use σ_w as the standard deviation to of W.

8. Autocorrelation functions for DLS results

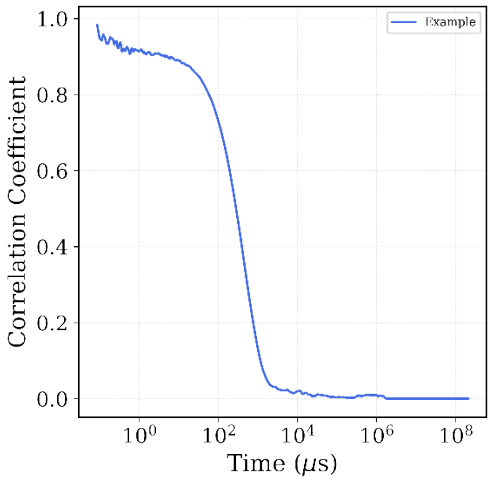

Fig S6. Autocorrelation functions for Fig 1C.

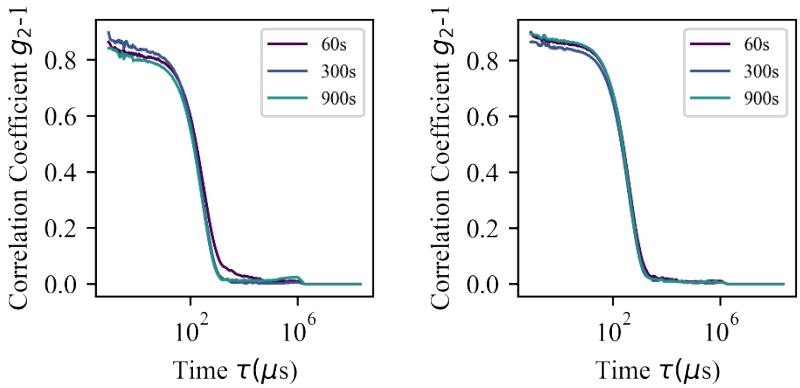

Fig S7. Autocorrelation functions for Fig 5A PE-Pristine (left), 5B PE-PFOA (right)

References cited

1. J. Almond, P. Sugumaar, M. N. Wenzel, G. Hill and C. Wallis, Determination of the carbonyl index of polyethylene and polypropylene using specified area under band methodology with ATR-FTIR spectroscopy, *E-Polym.*, 2020, **20**, 369–381.
2. B. Gewert, M. M. Plassmann and M. MacLeod, Pathways for degradation of plastic polymers floating in the marine environment, *Environ. Sci. Process. Impacts*, 2015, **17**, 1513–1521.
3. Y. Tang, K. Fan, I. Herath, W. Gustave, C. Lin, J. Qin and R. Qiu, Contribution of free hydroxyl radical to the formation of micro(nano)plastics and release of additives during polyethylene degradation in water, *Environ. Pollut.*, 2023, **337**, 122590.
4. D. Neibloom, M. A. Bevan and J. Frechette, Droplet Formation and Growth Mechanisms in Reaction-Induced Spontaneous Emulsification of 3-(Trimethoxysilyl) Propyl Methacrylate, *Langmuir*, 2021, **37**, 11625–11636.
5. M. Kerker, in *The Scattering of Light and Other Electromagnetic Radiation*, Elsevier, 1969, pp. 414–486.
6. J. W. T. Lichtenbelt, H. J. M. C. Ras and P. H. Wiersema, Turbidity of coagulating lyophobic sols, *J. Colloid Interface Sci.*, 1974, **46**, 522–527.
7. A. Y. Kim and J. C. Berg, Fractal Aggregation: Scaling of Fractal Dimension with Stability Ratio, *Langmuir*, 2000, **16**, 2101–2104.
8. X. Li, J. J. Lenhart and H. W. Walker, Aggregation Kinetics and Dissolution of Coated Silver Nanoparticles, *Langmuir*, 2012, **28**, 1095–1104.
9. K. L. Chen, S. E. Mylon and M. Elimelech, Aggregation Kinetics of Alginate-Coated Hematite Nanoparticles in Monovalent and Divalent Electrolytes, *Environ. Sci. Technol.*, 2006, **40**, 1516–1523.
10. B. V. Derjaguin, I. I. Abrikosova and E. M. Lifshitz, Direct measurement of molecular attraction between solids separated by a narrow gap, *Q Rev Chem Soc*, 1956, **10**, 295–329.
11. J. N. Israelachvili, in *Intermolecular and Surface Forces*, Academic Press Elsevier, 3rd edn., 2011, pp. 253–284.
12. J. C. Berg, in *An introduction to interfaces & colloids: the bridge to nanoscience*, World Scientific, 1st edn., 2010, pp. 525–613.
13. J. N. Israelachvili, in *Intermolecular and Surface Forces*, Academic Press Elsevier, 3rd edn., 2011, pp. 291–338.
14. B. Derjaguin, Untersuchungen über die Reibung und Adhäsion, IV, *Kolloid-Z.*, 1934, **69**, 155–164.
15. M. Moazzami-Gudarzi, G. Trefalt, I. Szilagyi, P. Maroni and M. Borkovec, Nanometer-ranged attraction induced by multivalent ions between similar and dissimilar surfaces probed using an atomic force microscope (AFM), *Phys. Chem. Chem. Phys.*, 2016, **18**, 8739–8751.
16. N. Ishida, K. Matsuo, K. Imamura and V. S. J. Craig, Hydrophobic Attraction Measured between Asymmetric Hydrophobic Surfaces, *Langmuir*, 2018, **34**, 3588–3596.